ORIGINAL RESEARCH

Combined Ibuprofen-Nanoconjugate Micelles with E-Selectin for Effective Sunitinib Anticancer Therapy

Xianhu Zeng[1], Yi Teng[1], Chunrong Zhu[2], Zhipeng Li [iD][1], Tian Liu[3], Yong Sun [iD][1], Shangcong Han [iD][1]

[1]Department of Pharmaceutics, School of Pharmacy, Qingdao University, Qingdao, People's Republic of China; [2]Department of Pharmacy Intravenous Admixture Service, Weifang Maternal and Child Health Hospital, Weifang, People's Republic of China; [3]Department of Urology, The Affiliated Hospital of Qingdao University, Qingdao, People's Republic of China

Correspondence: Shangcong Han; Yong Sun, Department of Pharmaceutics, School of Pharmacy, Qingdao University, Qingdao, People's Republic of China, Tel/Fax +86 532 82991508, Email hsc00111@163.com; sunyong@qdu.edu.cn

Introduction: Sunitinib, a first-line therapy with a certain effect, was utilized in the early stages of renal cell carcinoma treatment. However, its clinical toxicity, side effects, and its limited bioavailability, resulted in inadequate clinical therapeutic efficacy. Building neoteric, simple, and safe drug delivery systems with existing drugs offers new options. Therefore, we aimed to construct a micelle to improve the clinical efficacy of sunitinib by reusing ibuprofen.

Methods: We synthesized the sialic acid-poly (ethylene glycol)-ibuprofen (SA-PEG-IBU) amphipathic conjugate in two-step reaction. The SA-PEG-IBU amphiphilic conjugates can form into stable SPI nanomicelles in aqueous solution, which can be further loaded sunitinib (SU) to obtain the SPI/SU system. Following nanomicelle creation, sialic acid exposed to the nanomicelle surface can recognize the overexpressed E-selectin receptor on the membrane of cancer cells to enhance cellular uptake. The properties of morphology, stability, and drug release about the SPI/SU nanomicelles were investigated. Confocal microscopy and flow cytometry were used to assess the cellular uptake efficiency of nanomicelles in vitro. Finally, a xenograft tumor model in nude mice was constructed to investigate the body distribution and tumor suppression of SPI/SU in vivo.

Results: The result showed that SPI nanomicelles exhibited excellent tumor targeting performance and inhibited the migration and invasion of tumor cell in vitro. The SPI nanomicelles can improve the accumulation of drugs in the tumor site that showed effective tumor inhibition in vivo. In addition, H&E staining and immunohistochemical analysis demonstrated that the SPI/SU nanomicelles had a superior therapeutic effect and lower biotoxicity.

Conclusion: The SPI/SU nanomicelles displayed excellent anti-tumor ability, and can suppress the metastasis of tumor cell by decreasing the expression of Cyclooxygenase-2 due to the ibuprofen, providing an optimistic clinical application potential by developing a simple but safe drug delivery system.

Keywords: kidney cancer, nanomicelles, sialic acid, sunitinib, ibuprofen, anti-tumor therapy

Introduction

Renal carcinoma is the second most commonly occurring urinary system malignancy, which is classified pathologically as clear cell carcinoma, papillary cell carcinoma, and chromophobe cell carcinoma.[1,2] Among them, renal clear cell carcinoma accounts for about 70% to 75% of all renal malignancies. Radiotherapy, traditional chemotherapy, immunotherapy, and other therapeutic ways showed poor effects in patients with postoperative recurrence or metastasis of kidney cancer, whereas the emergence of targeted drugs has shown significant therapeutic benefits.[3,4]

Sunitinib is a multi-target tyrosine kinase inhibitor that inhibits the vascular endothelial factor receptors (VEGFR1-3), stem cell growth factor (c-Kit), platelet-derived growth factor receptor (PDGFR), and other signaling pathways to exert anti-tumor activity.[5] It is presently the standard of care for those individuals who suffer from metastatic renal cell carcinoma and have not been treated with prior therapy.[6–8] Although sunitinib is the drug of choice for recurrence and metastatic renal clear cell carcinoma by oral form, more than 60% of the dose is excreted from the body in the form of feces resulting in low bioavailability.[9,10] Moreover, sunitinib causes a variety of adverse reactions in clinical practice, including stimulation of the

gastrointestinal tract following the production of diarrhea, vomiting, and hand-foot syndrome (HFS) as well as white hair,[11,12] and more seriously, the damage to leucocytes and platelets.[13–15]

In order to increase the bioavailability and therapeutic effectiveness of sunitinib and reduce its unwanted side effects, drug carriers based on polymer conjugates and nanoparticles have been widely exploited.[16,17] Polymeric micelle is an ideal carrier system for the development of anticancer nanomedicines as it is customized to encapsulate drugs at doses used in clinical practice and tailored to achieve prolonged circulation kinetics necessary for tumor accumulation.[18–20]

Several studies have found significant correlations between tumor microenvironmental secretory factors and tumor progression, particularly related enzymes, growth factors and inflammatory factors have an impact on multiple aspects of tumor development.[21] Cyclooxygenase-2 (COX-2) is an inducible enzyme which is highly expressed in response to tissue injury and inflammation, causing pain and other symptoms.[22,23] Additionally, the increase of COX-2 has also been detected in a variety of malignancies, such as endometrial cancer,[24] colon cancer,[25,26] and prostate cancer,[27] showing evidence that COX-2 can contribute to tumorigenesis and metastasis.[28–30] Besides, prostaglandins (PGs) catalyzed by COX-2 have proven to promote tumor growth and metabolism.[31] In conclusion, COX-2 was considered as a potential therapeutic target for cancer treatment.[32]

Ibuprofen, a nonsteroidal anti-inflammatory drug (NSAID),[33] is extensively used to decrease COX-2 production.[34] Surprisingly, ibuprofen has been proven to show some efficacy in the treatment of cancer, which is a classic case of "old drug new tricks". In this research, we synthesized the sialic acid-poly (ethylene glycol)-ibuprofen (SA-PEG-IBU) amphipathic conjugate which can self-assemble into nanomicelles and load sunitinib in aqueous solution. Sialic acid (SA) is a derivative of neuraminic acid,[35,36] which can specifically target to E-selectin receptors. Our prior research established that overexpression of E-selectin provides a biological basis for targeting renal cancer cells in the tumor microenvironment (Supporting Figure S1). Under the mediating effect of tumor targeting, the sunitinib loaded SA-PEG-IBU nanomicelles (SPI/SU) were precisely delivered to the tumor site, simultaneously releasing both sunitinib and ibuprofen. Briefly, the SPI/SU nanomicelle demonstrated substantial antitumor activity and decreased toxicity compared with free sunitinib. This research will provide a brand-new perspective on the existing combo therapy: new drug delivery platform incorporating conventional pharmaceuticals will play a new role in anti-cancer, providing a possible field of exploration to construct the medication delivery platform.

Material and Methods
Synthesis of Sialic Acid-Poly (Ethylene Glycol)-Ibuprofen (SA-PEG-IBU)

The SA-PEG-IBU conjugates (SPI) were synthesized via a two-step reaction. Firstly, ibuprofen was conjugated to HOOC-PEG-NH$_2$ by amidation. In brief, in anhydrous dimethyl sulfoxide (DMSO), 21 mg ibuprofen was entirely dissolved. The carboxyl groups on ibuprofen were activated using EDC and NHS, and the mixed solution was agitated constantly for 2 hours.[37], 200 mg PEG was thoroughly dissolved in 2 mL DMSO using an ultrasonic bath and then gently dripped into the reaction solution described above, stirring continuously to allow the reaction to proceed overnight at room temperature. Following the reaction, the HOOC-PEG-IBU grafts (PI) were obtained after purifying the reaction solution for 48 hours in deionized water and freeze-drying. The PI conjugates were collected and weighed to determine the yield. Secondly, 100 mg PI was dissolved in 10 mL DMSO, and EDC and 4-DMAP were added to accelerate the carboxyl group activation for 2 hours, Similarly, the DMSO solution of SA was gradually added after entirely dissolved, and the reaction was carried out overnight at room temperature.[38] SPI conjugates were lyophilized and weighed to calculate the final yield. All of these reactions take place under the protection of nitrogen. The structures of the reactants and products were verified by FT-IR spectrometer and ^{1}H NMR, respectively.

Preparation and Characterization of Sialic Acid-Poly (Ethylene Glycol)-Ibuprofen (SPI) Nanomicelles

1 mg of the lyophilized SA-PEG-IBU conjugate was dispersed in water by ultrasonic for 10 mins to allow the SA-PEG-IBU conjugate to fully self-assemble into nanomicelles. To prepare the SPI/SU drug loaded nanomicelles, the SPI and sunitinib were dissolved in 1 mL DMSO, then the DMSO solution was gradually added to 10 mL deionized water (containing 1.25 μL triethylamine) drop by drop under stirring.[39] The mixed solution was agitated overnight and then dialyzed against deionized water for 24 h and finally freeze-dried to obtain the SPI/SU lyophilized powder.

The size and zeta potential of the SPI nanomicelle and SPI/SU nanomicelle were measured by dynamic light scattering (Nano-ZS90, Malvern Zetasizer, UK), and the morphology of different nanomicelles were visualized using TEM (JSM-6490LA, JEOL, JAPAN).[40] To evaluate the stability of the SPI nanomicelle, the particle size of SPI nanomicelle in PBS and complete medium were measured for 7 days, respectively.

To investigate the drug loading efficiency, 1 mg SPI/SU nanomicelle was weighed and dissolved in DMSO. The absorbance at wavelength 444.4 nm was measured by UV spectrophotometer (UV-2600, SHIMADZU, JAPAN) and substituted into the standard curve of sunitinib to calculate the loading capacity (LC) and encapsulation efficiency (EE), respectively.[41] The loading capacity and encapsulation efficiency were calculated as follows:

$$LC(\%) = \frac{\text{Weight of sunitinib in nanoparticles}}{\text{Weight of nanoparticles}} \times 100\%$$

$$EE(\%) = \frac{\text{Weight of sunitinib in nanoparticles}}{\text{Weight of sunitinib added}} \times 100\%$$

Evaluation of Drug Release Using an Ultraviolet-Visible Spectrophotometer

1 mg of SPI/SU nanomicelles suspended, respectively, 1 mL of PBS were sealed in dialysis bag (MWCO 3.5 kDa) and then immersed in 30 mL PBS with pH at 7.4, 6.8 and 5.5 containing 0.5% Tween-80 to evaluate the sunitinib release.[42] At the designed time interval (0.5, 1, 2, 4, 8, 12, 24 and 48 h), 3 mL of the release solution including 5 units of esterase was taken out and the corresponding volume of new PBS was added. All the above drug release behaviors were carried out at 100 rpm on a shaker at 37°C, which was shielded from light. The released sunitinib was quantified by UV spectrophotometer at the wavelength of 444.4 nm. The drug release of ibuprofen was also carried out under the same conditions as above, and the content of ibuprofen was detected at the wavelength of 265.0 nm.[43]

Detection of Cytotoxicity on 293T, 786-O and ACHN Cell Lines

The cytotoxicity of SPI nanomicelles to 293T, 786-O, and ACHN cells were assessed by MTT assay. The 293T, 786-O, and ACHN cells were seeded into 96-well plates at a density of 5×10^3 cells per well and then cultured for 24 h. The nanomicelles were distributed in serum-free media at gradient concentrations (0.01–2 mg/mL) and cultured with the cells for 24 hours. 5 mg/mL MTT solution was immediately added each well and incubated at 37°C for another 4 hours.[44] After removing the medium from each well, 200 μL DMSO was added and agitated for 15 minutes. Absorption at 490 nm was measured using microplate reader (Infinite F200 PRO, TECAN, AUSTRIA).

Measurement of Cellular Uptake on 786-O and ACHN Cell Lines

786-O, ACHN cells were seeded in glass bottom cell culture dishes (1×10^4 cells/dish), respectively.[45] After overnight incubation, the culture medium was replaced by fresh serum-free medium containing SPI/5-FAM, PI/5-FAM nanomicelles at a concentration of 1 mg/mL. Herein, 5-FAM (Ex/Em: 490 nm/520 nm) was used as a mimic of sunitinib and the loading method is same as sunitinib. After incubation for 2 h, 4 h at 37°C, cells were washed with PBS and fixed with 4% paraformaldehyde for 30 min. The cytoskeleton was stained with Actin-Tracker Red-Rhodamine (Ex/Em: 544 nm/576 nm) for 45 min after being washed with PBS containing 0.1% Triton X-100, and nuclei were then stained by DAPI (Ex/Em: 340 nm/488 nm) for 5 min. Cells were washed with PBS for three times, and the cellular uptake were observed via confocal laser scanning microscopy (STELLARIS 5, Leica, GERMANY).

Cellular uptake efficiency of nanomicelles was also quantified by flow cytometry (FCM). 786-O, ACHN cells were treated in 6-well plates (3×10^5/well) with SPI/5-FAM, PI/5-FAM nanomicelles as described above the concentration of nanomicelles for 2 and 4 h, cells were collected and resuspended in 500 μL cold PBS for flow cytometry analysis with CytoFLEX S (Beckman Coulter, USA).

Detection of Migration and Invasion by Wound Healing Assay and Transwell Assay

786-O, ACHN cells were, respectively, cultured in 6-well plates for 24 hours until the cell density of more than 80% per well. Serum-free cell culture medium is selected to restrict excessive proliferation of cell. Each well was striated by a sterile pipette tip, and the floating cells were then washed away with PBS. The cells were incubated in different experimental groups for 24 h at 37°C in a humidified 5% CO_2 atmosphere. The width of wound was observed using Olympus IX53 microscope (Olympus, JAPAN). The cell migration rate was calculated by Image J software.

The cells invasion inhibition was assessed with transwell assay.[46] In brief, the cultured 786-O and ACHN cells were harvested and resuspended at a density of $5×10^5$/mL in serum-free medium. 600 μL serum-supplied medium was added to the 24-well plate containing the transwell chamber, 100 μL cell suspension and 100 μL medium containing various drug formulations were put into the transwell chamber for 24 h. Afterwards, the cells were fixed with 4% paraformaldehyde and stained with 0.1% crystal violet (w/v, diluted with PBS). The cells on the upper chamber were removed gently with cotton swab. The migrant cells on the bottom of chamber were observed and counted via microscope.

Western Blot Analysis of Cyclooxygenase-2 Protein

786-O cells and ACHN were, respectively, cultured in 6-well plates to a density of $1×10^6$ cells/well. The cells were collected after treating with SPI/SU, PI/SU, and SPI nanomicelles, SU, IBU, and PBS for 24 h. Protease inhibitor-containing cell lysates were added to cell-culture dish for lysing on ice. Centrifugation at 12,000 RPM for 15 minutes at 4°C, followed by absorption of the supernatant for protein measurement using a BCA protein assay kit. The proteins were heated at 95 °C in the metal bath for 10 minutes before being stored at −80°C.

Each group was sampled with 10 μg protein, separated on a 10% sodium dodecyl sulfate-polyacrylamide (SDS-PAGE) gel, then transferred to a polyvinylidene difluoride (PVDF) membrane. At room temperature, the PVDF bands were incubated with blocking reagent for 2 hours and washed three times with TBST for 5 minutes each. Then, the PVDF bands were treated overnight with primary antibodies against COX-2 and GAPDH at 4°C, respectively. The membrane strip and secondary antibody labeled with HRP were incubated for 1 hour at room temperature. Immunoreactivity were detected with ECL substrates and viewed through a WB imaging equipment (BIO-RAD ChemiDoc™ XRS+, USA), and the gray value was evaluated using Image J software.

Observation of Biodistribution by Infrared Imaging System

To observe the biodistribution of the SPI nanomicelles, tumor-bearing mice were intravenously injected with DiR-loading SPI nanomicelles and free DiR (Ex/Em: 750 nm/780 nm). The biodistribution of nanomicelles in vivo was observed via an infrared imaging technique at determined time points (3, 6, 12, 24 h) after administration. Then, mice were sacrificed to isolate the major organs and tumors. The fluorescence intensity photographs of isolated organs were taken using an infrared imaging system (IVIS Spectrum, USA).

Detection of Antitumor Efficacy Study on Subcutaneous Tumor Model

BLAB/c nude mice (5–6 weeks old) bearing tumors were used to evaluate the antitumor efficacy about various drug groups. 786-O cell suspension ($2×10^6$ cells/0.1mL) was subcutaneously injected into the right posterior groin of the mice. The mice were randomly divided into six groups (n=4 for each group) when the tumors reached 100 mm^3. The six groups were injected with (1) SPI/SU, (2) SU, (3) PI/SU, (4) IBU, (5) SPI, (6) Saline via tail vein for once three days, seven times in total. Body weight and tumor volumes were recorded every three days throughout the experiment, and tumor volume was computed using the formula: tumor volume (mm^3) = (length×width^2)/2.[47] 22 days later, the tumor tissues and major organs were collected and fixed for subsequent histochemistry analysis.

Observation of Antitumor Efficacy and Safety by Histochemistry Analysis

Major organs and tumor were dissected to further evaluate the antitumor efficiency. H&E staining was used to study and compare the cell states of tumor tissues, while terminal deoxynucleotidyl transferase-mediated dUTP nick-end labeling (TUNEL) staining was used to analyze and compare the apoptosis of tumor tissues. Immunohistochemistry with Ki-67

indicated the proliferative state of the tumor cells. The expression of COX-2 was observed by immunofluorescence labeling (primary antibody: COX-2 Mouse Monoclonal antibody, secondary antibody: FITC-labeled Goat Anti-Mouse IgG), which revealed the inhibition effect of ibuprofen. All of sections were observed with an upright fluorescent microscope (Nikon Ni-U, JAPAN).

Statistical Analysis

All experimental data were presented as mean ± standard deviation (SD). Statistical analysis was performed with GraphPad Prism software package Version 8.0 (GraphPad, Inc., USA). Statistical significance was tested using a Student's t-test. A p-value < 0.05 was considered to represent statistical significance.

Results and Discussion

Synthesis of Sialic Acid-Poly (Ethylene Glycol)-Ibuprofen (SA-PEG-IBU)

The synthesis routes of PEG-IBU (PI) conjugate and SA-PEG-IBU (SPI) conjugate were shown in Figure S2. Briefly, ibuprofen and PEG were amidated in the first step of the reaction, and the final SPI conjugate was a product of the esterification of sialic acid with the first reaction product. The structures of the products were verified by ^{1}H NMR and FT-IR. ^{1}H NMR spectrum (Figure 1A) of the conjugate of SA-PEG-IBU was referred to the ^{1}H NMR spectra (Supporting Figure S3) of HOOC-PEG-NH$_2$ and HOOC-PEG-IBU, the characteristic peaks corresponding to SA-PEG-IBU conjugate were as below: 0.85 ppm (CH$_3$CHCH$_3$, 6H), 7.09–7.19 ppm (Benzene ring, 4H), 8.06–8.08 ppm (-NH-CO-, 1H). Furthermore, Figure 1B presents the FT-IR spectra of PEG, PEG-IBU and SA-PEG-IBU conjugates. The PEG-IBU presented characteristic absorption bands at 1549 cm^{-1} belonging to CO-NH-, in agreement with the successful coupling of PEG and IBU. Consequently, combining the ^{1}H NMR with the infrared spectrum led to the conclusion that it had been demonstrated that the SA-PEG-IBU conjugates were successfully synthesized.

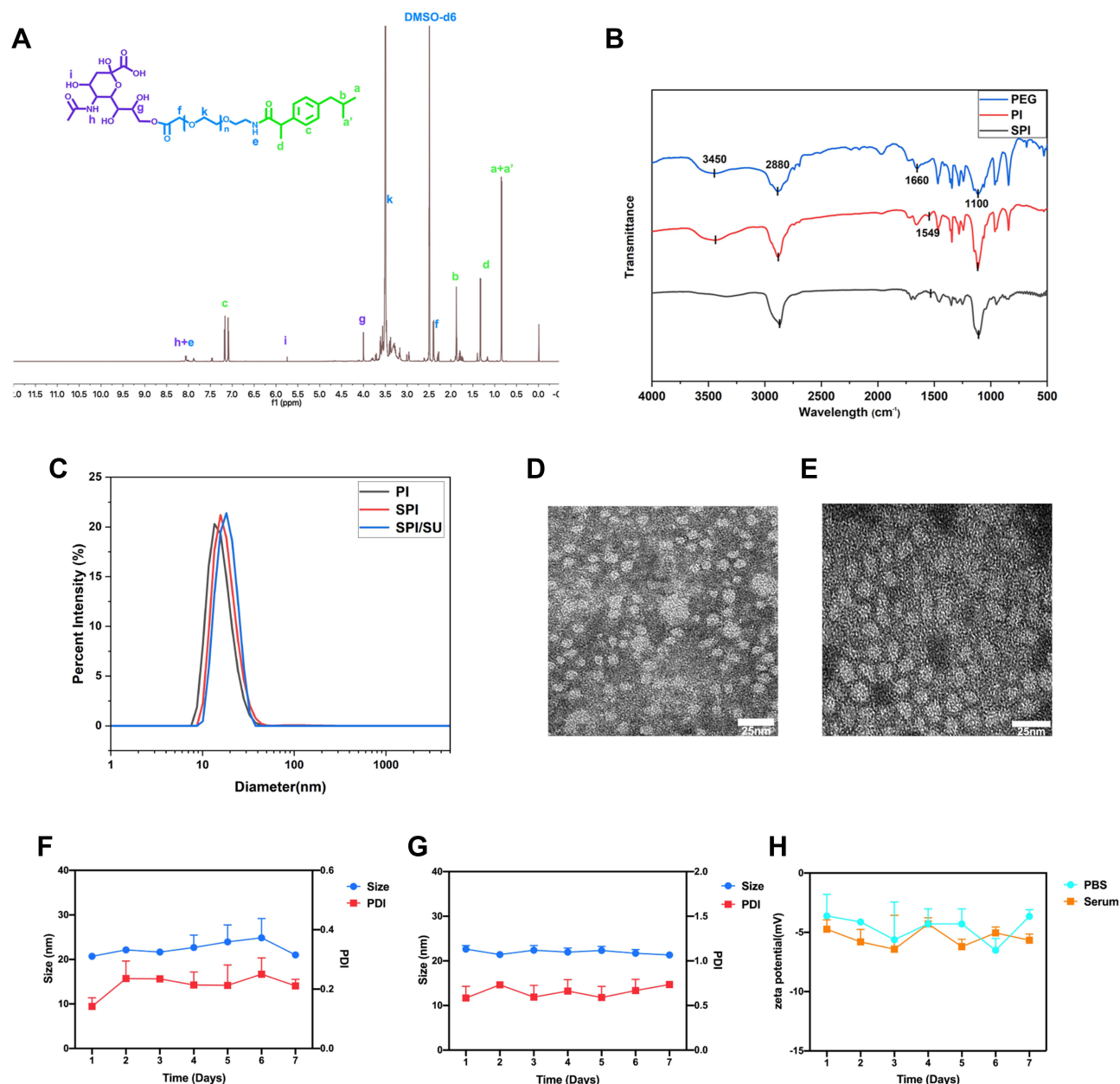### Characterization of Sialic Acid-Poly (Ethylene Glycol)-Ibuprofen (SPI) Nanomicelles

SPI conjugates can self-assemble into nanosized micelles in aqueous solution, and the critical micelle concentration (CMC) was measured at 0.021 mg/mL (Supporting Figure S4). The particle size and zeta potential of nanomicelles were determined by DLS, and the morphology was observed by TEM. As shown in Figure 1C, the diameter of SPI, PI and SPI/SU nanomicelles were 18.53 ± 0.12 nm, 13.17 ± 0.14 nm, 21.42 ± 0.25 nm, respectively. It can be seen that the particle size of SPI/SU nanomicelles rose slightly after loading sunitinib, but remained within a narrow particle size distribution. Furthermore, these nanomicelles showed excellent stability after lyophilization. PI can also form nanomicelles with approximate particle size, we utilized PI as a negative control with no targeting property. Meanwhile, TEM revealed a consistent sphere in the particle size shape as shown in Figure 1D and E.

The particle size and zeta potential of nanomicelles did not change significantly in PBS and 10% serum, nor did the value of the particle distribution index (PDI), as shown in Figure 1F–H. Drug loading capacity (LC) and encapsulation efficiency (EE) of SPI/SU nanomicelles with different SPI/sunitinib ratios were evaluated to obtain a satisfactory SPI/ sunitinib ratio of 10:1. Under this circumstance, the LC and EE of the SPI/SU nanomicelles were 8.3% and 91.3%, respectively (Table 1).

The Property of Drug Release in vitro

The release properties of sunitinib in vitro were investigated at different pH (7.4, 6.8 and 5.5) to mimic the condition of physiological pH and tumor sites, respectively. Sunitinib released rate gradually slowed down within 8 h under various pH circumstances (as shown in Figure 2A). At pH 7.4, the total cumulative release of sunitinib was slightly lower than in the other two conditions, implying that SPI/SU nanomicelles could more efficiently release sunitinib in the tumor microenvironment.

The SPI/SU nanomicelles exhibited faster release at pH 6.8 and 5.5. Roughly 35.7% of ibuprofen was released at pH7.4 within 8 h, whereas ibuprofen release was around 77.1% and 64.8% at pH 6.8 and 5.5, respectively (As shown in Figure 2B). The release of ibuprofen was ineffective in the physiological pH environment of 7.4, but it was relatively efficient in the simulated tumor microenvironment and the internal endosome and lysosome. The release rate of ibuprofen

Figure 1 Physicochemical characterization and stability of SPI nanomicelles. (**A**) ^{1}H NMR spectra of SA-PEG-IBU in d6-DMSO. (**B**) IR spectra of PEG (HOOC-PEG-NH$_2$), PEG-IBU, SA-PEG-IBU. (**C**) Size distribution of blank PI nanomicelles, SPI nanomicelles and SPI/SU nanomicelles. (**D**) TEM image of SPI nanomicelles (scale bar = 25 nm). (**E**) TEM image of SPI/SU nanomicelles (scale bar = 25 nm). (**F**) Particle size distribution and PDI of SPI nanomicelles in PBS at 7 days, n=3. (**G**) Particle size distribution and PDI of SPI nanomicelles in 10% serum for 7 days, n=3. (**H**) Zeta potential distribution of SPI nanomicelles in PBS and 10% serum within 7 days, n=3. All data are means ± SD.

declined after 12 hours, which we thought might be connected to the progressive esterase inactivation. Ibuprofen can be delivered efficiently at the tumor site and perform a therapeutic role attributed to the mediating of pH and enzyme activity.

Cytotoxicity of Sunitinib-Loaded Nanomicelles to 293T, 786-O and ACHN Cell Lines

MTT assay was used to evaluate the toxicity of the SPI nanomicelles on HEK 293T, 786-O, and ACHN cell lines. The cellular toxicity of the SPI nanomicelles exhibited concentration-dependent behavior in all three cell lines (Figure 2C). It is worth noting that higher cytotoxicity in 786-O and ACHN cells were observed. This could be due to increased

Table 1 The Loading Capacity and Encapsulation Efficiency Rates of SPI/SU Nanomicelles and Sunitinib Drugs at Different Mass Ratios

Sunitinib Mass (mg)	SPI Mass (mg)	LC (%)	EE (%)
0.5mg	10mg	4.6%	97.2%
1.0mg	10mg	8.3%	91.3%
1.5mg	10mg	8.2%	62.8%
2.0mg	10mg	7.2%	43.2%

expression of E-selectin receptors on the surface of 786-O and ACHN cells, which facilitated and mediated the uptake of SPI nanomicelle, resulting in increased cytotoxicity.

As depicted in Figure 2D, SPI/SU nanomicelles showed efficient cytotoxicity to tumor cells at a particular concentration and similar therapeutic tendencies in different tumor cells. The hemolysis of the SPI material was also tested. As expected, there was no obvious hemolysis reaction while it was at high concentrations (Supporting Figure S5). These results showed that the SPI material has good biocompatibility.

Cellular Uptake in 786-O and ACHN Cell Lines

The cellular uptake of SPI and PI nanomicelles in 786-O (Figure 3A) and ACHN cells (Figure 3D) were observed by confocal microscopy. As expected, a stronger 5-FAM fluorescence signal was detected in the SPI group compared
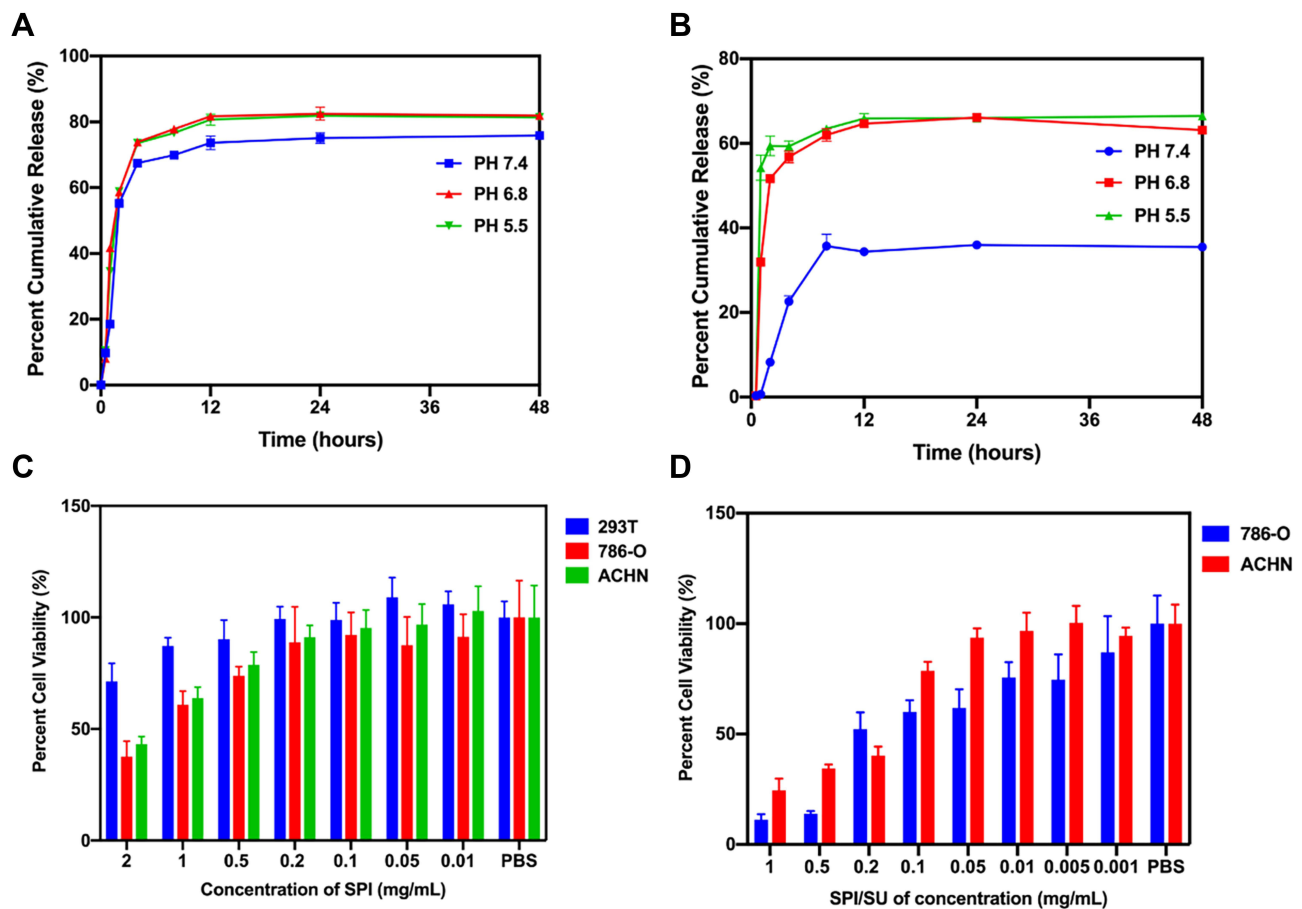

Figure 2 Drug release properties and cytotoxicity of nanomicelles. (**A**) The cumulative drug release amounts of sunitinib in PBS at pH7.4, 6.8, and 5.5, (n=3). (**B**) The cumulative drug release amounts of ibuprofen in PBS at pH 7.4, 6.8, and 5.5, (n=3). (**C**) The cytotoxicity of SPI blank nanomicelles to 293T, 786-O and ACHN cells at different concentrations, (n=6). (**D**) The cytotoxicity of SPI/SU nanomicelles to 786-O and ACHN cells at various the concentrations of sunitinib, (n=6).
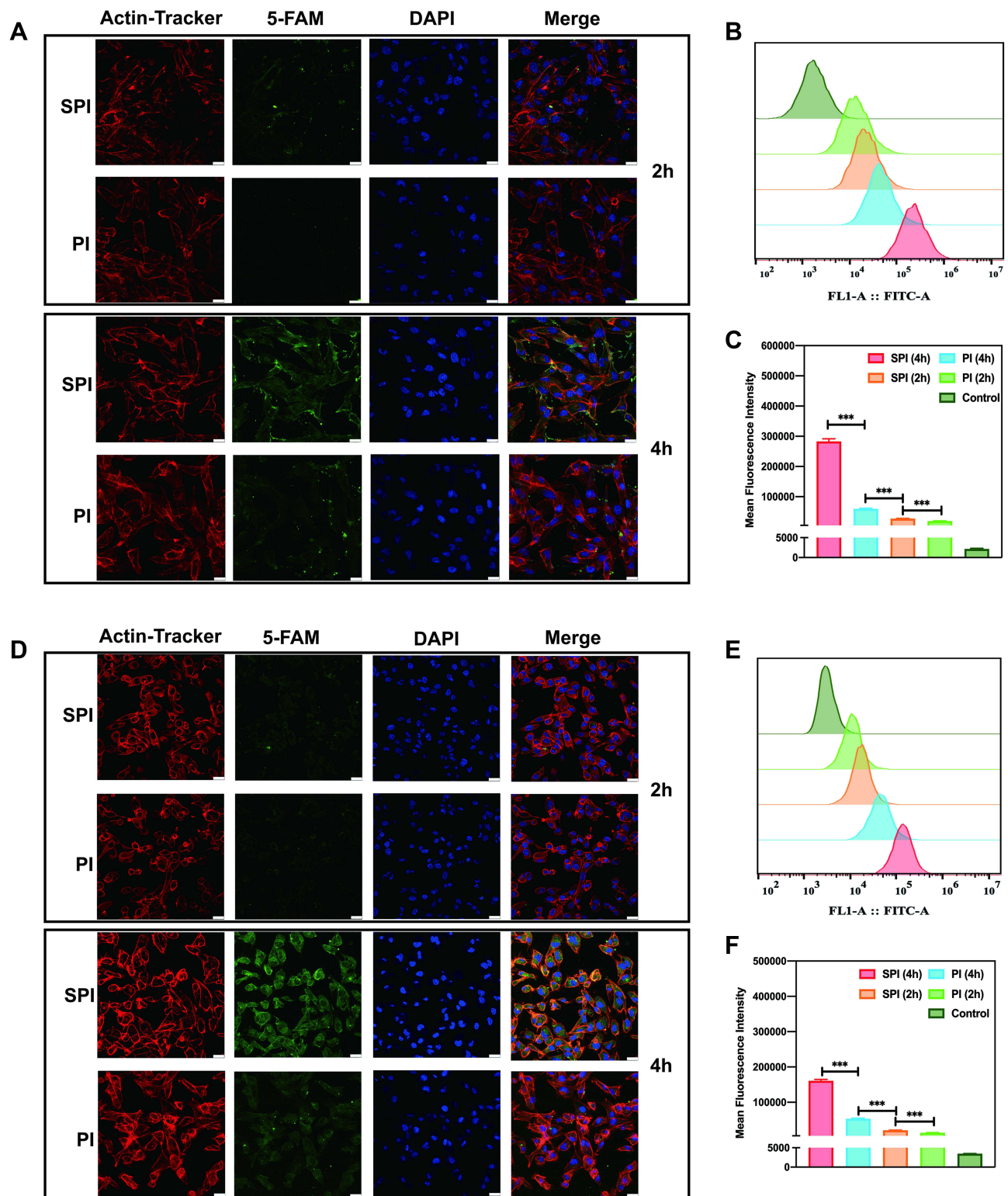
Figure 3 In vitro cellular uptake of SPI nanomicelles in 786-O and ACHN tumor cell lines. (**A**) The Confocal microscope image of 786-O cell lines after incubation with SPI nanomicelles and PI nanomicelles for 2 h and 4 h, respectively. The scale bar is 25 μm. (**B**) Flow cytometric determination of SPI nanomicelles and PI nanomicelles uptake in 786-O cell lines. (**C**) The fluorescence intensity of 786-O cell micellar uptake was quantified by flow cytometry. (**D**) The Confocal microscope image of ACHN cell lines after incubation with SPI nanomicelles and PI nanomicelles for 2 h and 4 h, respectively. The scale bar is 25 μm. (**E**) Flow cytometric determination of SPI nanomicelles and PI nanomicelles uptake in ACHN cell lines. (**F**) The fluorescence intensity of ACHN cell micellar uptake was quantified by flow cytometry. All data are means ± SD, n=3. ***p < 0.001.

with the PI group in both cell lines, indicating that the SA group can promote the endocytosis mediated by the E-selectin receptor, which is consistent with the experimental results of cytotoxicity assay.

To quantify micelle accumulation, the intracellular fluorescence intensity of the SPI (Figure 3B and C) and PI groups (Figure 3D and F) was detected by flow cytometry, which was consistent with that of confocal microscopy analysis. In the PI group, the fluorescence intensity decreased compared with the SPI group within 2 hours. By contrast, higher amounts of the fluorescence signal were detected within 4 hours, which showed that SA-modified micelles increased the drug uptake in a time-dependent manner. Moreover, the f-actins were labeled by Rhodamine to evaluate the reorganization of the cellular cytoskeleton in both cell lines because abnormal damage to the cytoskeleton can influence some cell functions, including proliferation, apoptosis, adhesion and migration.[48–51] As a vital structural support for cell migration, the amount of pseudopodia dropped and contracted significantly following ingestion of the SPI nanomicelles, which may be a significant factor in the suppression of tumor cell metastasis (Supporting Figure S6).

Migration and Invasion in 786-O and ACHN Cell Lines

To evaluate tumor cell migration after medication treatment, wound healing assays were performed. Following the scratches, the 786-O and ACHN cells were imaged at 0 h and 24 h following drug incubation. The cell migration rates were calculated using Image J software. In comparison with the control group, other experimental groups showed inhibition of cell migration at varying degrees (as shown in Figure 4A). Particularly, the SPI/SU group and the sunitinib group inhibited 786-O cells more effectively at the approximate level (Figure 4C). Similarly, the SPI/SU group and the sunitinib group also showed the best inhibition of cell migration among all experimental groups in ACHN cells, although the inhibition level was lower than that of 786-O cells (Figure 4D). Additionally, the ibuprofen-free drug group demonstrated slight suppression of migration, which was also found with blank nanomicelles. This result showed that it may be related to the inhibition of COX-2 by ibuprofen.[52]

Transwell migration experiments could be used to evaluate the longitudinal motility of cells, reflecting the invasion ability of tumor cells to a certain extent. The migrant cells on the bottom of chamber were imaged and counted 24 hours after seeding. The result of the transwell assay indicated that it had a similar inhibitory effect as the above-mentioned result. In comparison to the control group, tumor cell metastasis was milder in the treatment group (Figure 4B). More notably, SPI/SU had a considerable inhibitory effect on 786-O cells (Figure 4E) and ACHN cells (Figure 4F), even stronger than the sunitinib group.

Interaction of COX-2 with its specific EP receptors on the surface of cancer cells has been proved to induce cancer migration and invasion.[53] To verify whether inhibition of COX-2 by ibuprofen in SPI nanomicelles affected the migration and invasion ability of tumor cells, the expression of COX-2 was measured in each experimental group of 786-O (Figure 5A) and ACHN cell lines (Figure 5B) by Western Blot assays. The results showed that the SPI/SU and ibuprofen groups exhibited lower expression than the other groups, which consistent with the experimental results above (Figure 5C and D). However, it is noteworthy that the significant inhibition of cell migration was observed with sunitinib but at a high level of COX-2 expression, which revealed the inhibition of cell migration of sunitinib might exert through other mechanisms. The results demonstrated that the SPI/SU nanomicelles may suppress the migration and invasion abilities of tumor cells by down-regulating COX-2 with ibuprofen; meanwhile, the targeted delivery of sunitinib enhanced its therapeutic effect.

Biodistribution and Antitumor Efficacy on Subcutaneous Tumor Model

DiR was loaded into SPI nanomicelles as a mimic of sunitinib to track the biodistribution. As shown in Figure 6A, SPI nanomicelles showed enhanced accumulation in the tumor from 3 to 24 h. The tumor tissues and main other organs were harvested and imaged ex vivo. As shown in Figure 6B, the fluorescence signal of SPI/DiR nanomicelles in tumor tissues was much stronger than that of free DiR, indicating an ideal tumor-targeting capacity of SPI nanomicelles. It can also be seen that strong signal were detected in spleen, which may be attribute to the increased expression of E-selectin in the spleen to respond to the inflammatory in the tumor.[54]
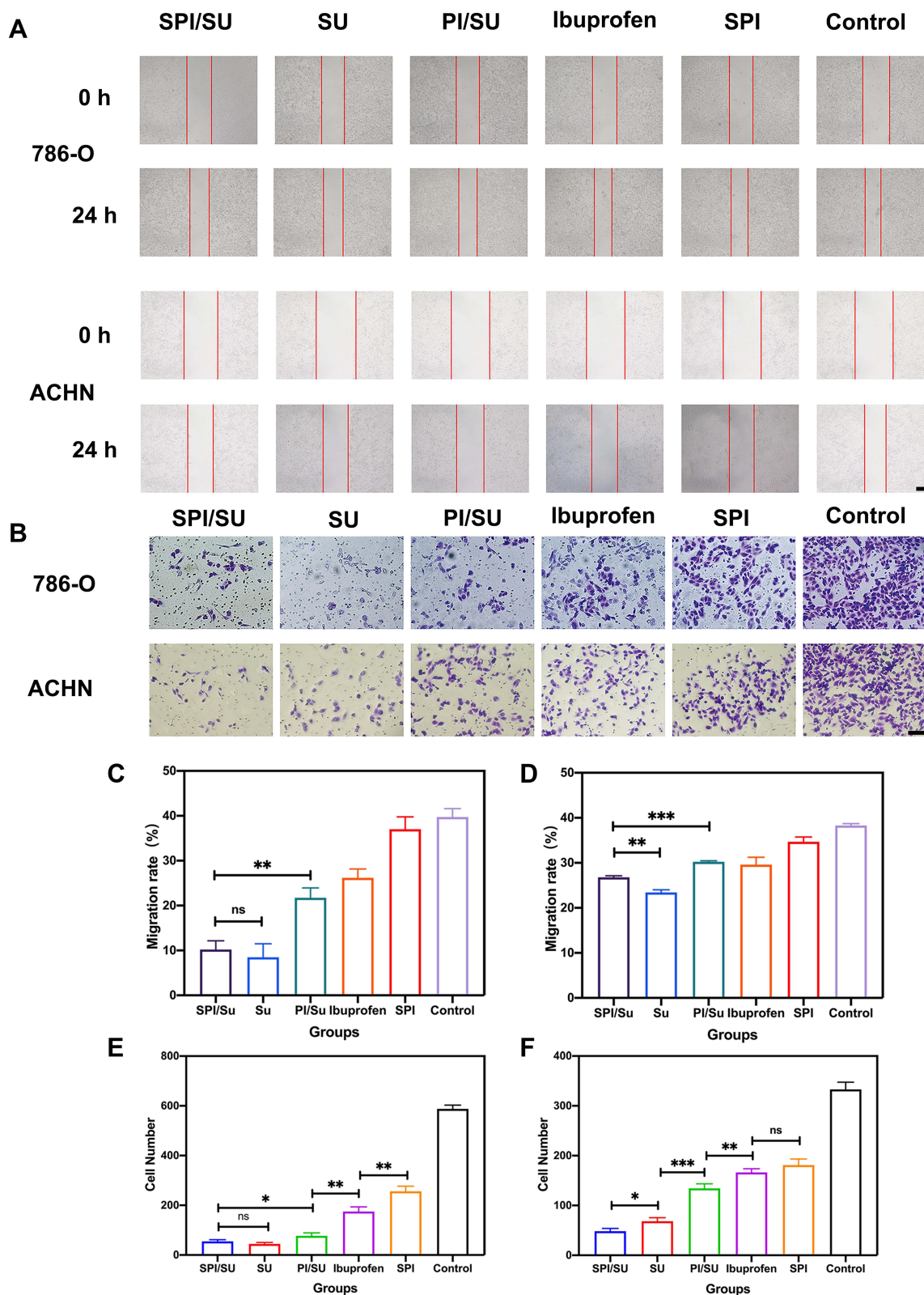
Figure 4 In vitro wound healing activity and transwell assay of SPI nanomicelles. (**A**) Wound healing activity of 786-O and ACHN cell lines after treatment of SPI/SU, SU, PI/SU, ibuprofen, SPI, control group for 24 h. The scale bar = 200 μm. (**B**) Transwell activity of 786-O and ACHN cell lines after treatment of SPI/SU, SU, PI/SU, ibuprofen, SPI, control groups for 24 h. The scale bar = 50 μm. (**C** and **D**) Cell migration rate was calculated by ImageJ. (**E** and **F**) The cells were counted under a microscope and averaged. All data are means ± SD, n=3. *p < 0.05, **p < 0.01, ***p < 0.001.
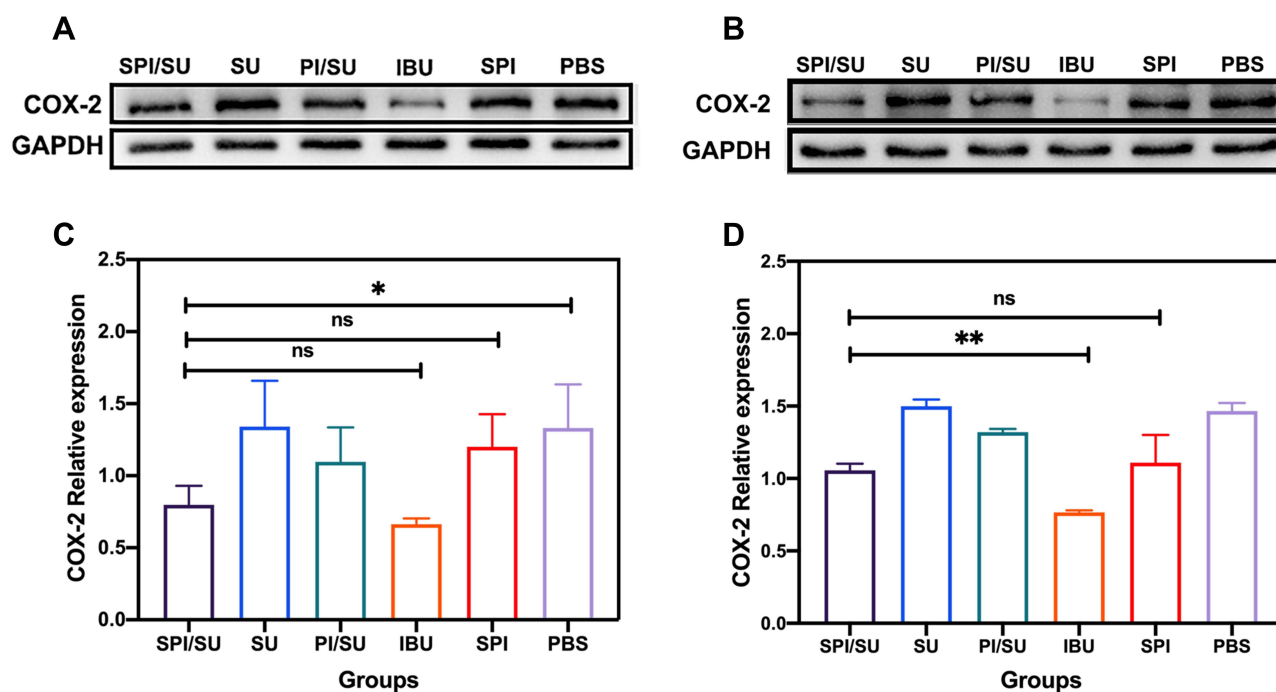**Abbreviation**: ns, not significant.

Figure 5 (**A**) The protein expression level of COX-2 in 786-O cells, treated with SPI/SU, SU, PI/SU, IBU, SPI, PBS for 24 h, GAPDH was used as endogenous reference. (**B**) The protein expression level of COX-2 in ACHN cells, treated with SPI/SU, SU, PI/SU, IBU, SPI, PBS for 24 h, GAPDH was used as endogenous reference. (**C**) COX-2 relative expression was calculated by ImageJ in 786-O cells. (**D**) COX-2 relative expression was calculated by ImageJ in ACHN cells. All data are mean ± SD, n=3. *$p < 0.05$, **$p < 0.01$. **Abbreviation**: ns, not significant.

The tumor treatment efficacy was investigated in the tumor-bearing nude mice models. As shown in Figure 6C–E, each group of SPI/SU, PI/SU, free sunitinib and free ibuprofen showed a tumor inhibition rate of more than 50%. Strikingly, SPI/SU nanomicelles inhibited tumor growth the most effectively, with an average tumor inhibition rate at 84%. Although the free sunitinib group also showed positive tumor inhibition, the body weight loss could not be ignored (Figure 6F), suggesting a systemic side effect or cachexia caused by free sunitinib might occur. Meanwhile, during the 21-day treatment period, no body weight loss was observed in SPI/SU group, demonstrating minimum side effects. Weight loss may be due to gastrointestinal irritation and blood toxicity of sunitinib itself, or cachexia caused by tumor progression. In brief, the SPI micellar delivery system increases drug enrichment at the tumor site to enhance the anti-tumor activity but reducing side effects.[51,55,56]

Histochemistry Analysis of Antitumor Efficiency and Biosafety

Histochemistry analysis of tumor tissues was further performed. As shown in Figure 7A and B, SPI/SU treatment group exhibit the fewest tumor cells and the most severe tumor necrosis in H&E stained sections. Meanwhile, SPI/SU treatment group also exhibit the lowest cell proliferation (stained by Ki67[57]) and the highest cell apoptosis (TUNEL assay[58]). Moreover, to check the expression of COX-2 for anti-metastasis, the tumor sections were stained by immunofluorescence. Consistent with the results of cell experiments, SPI/SU showed the strongest COX-2 down-regulation, indicating that SPI/SU can also inhibit tumor metastasis and invasion in vivo (Figure 7C). However, the ibuprofen treatment group did not show the same COX-2 down-regulation effect as the cell experiment. This may be because ibuprofen was difficult to be effectively enriched in the tumor site after tail vein injection, resulting in low drug concentration in the tumor tissue.

Main organs of all the tested nude mice were collected for H&E histopathology analysis to investigate the organ toxicity in vivo, which is important for the clinical application of drug delivery system.[59] The histopathology analysis revealed that the SPI/SU nanomicelles did not cause visible damage to main organs, including the heart, lung, liver, spleen, and kidney as shown in Figure 8A. Moreover, blood routine examinations were performed for each group. In comparison with free sunitinib, the SPI/SU nanomicelles showed significant alleviation of leukopenia and
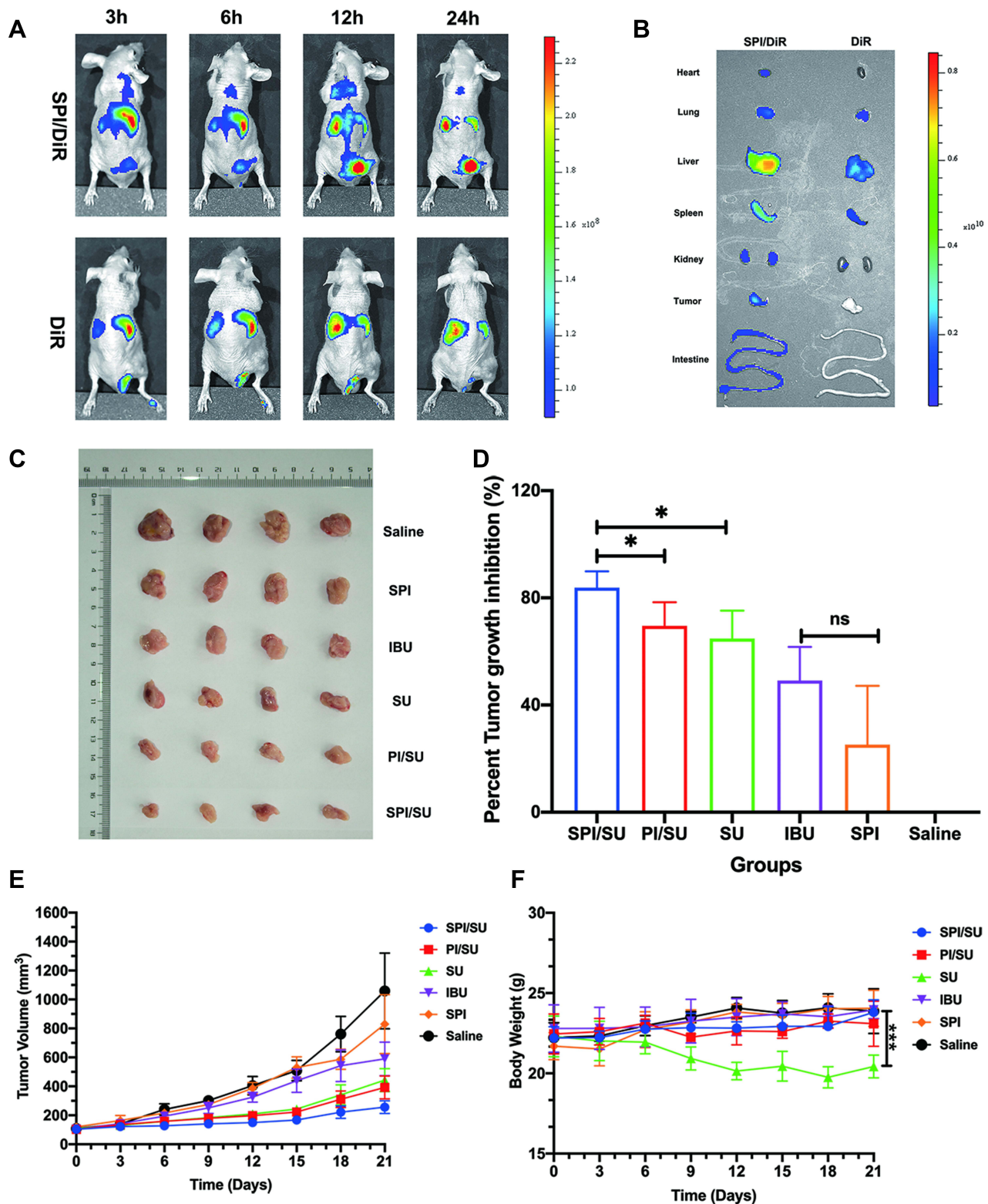
Figure 6 (**A**) In vivo biodistribution of SPI nanomicelles, mice treated with SPI/DiR nanomicelles and DiR solution via tail vein injection. (**B**) Ex vivo images of main organs or tumors excised from nude mice at 24 h after intravenous injection. (**C**) In vivo anti-tumor efficiency of different drug formulations in nude mice bearing 786-O xenograft tumors. Image of excised tumors at the end of the experiment. (**D**) Tumor growth inhibition rate. (**E**) Tumor growth curve. (**F**) The changes in body weight of nude mice. The error bars represent standard deviation (n=4). All data are mean ± SD, n=3. *$p < 0.05$, ***$p < 0.001$.
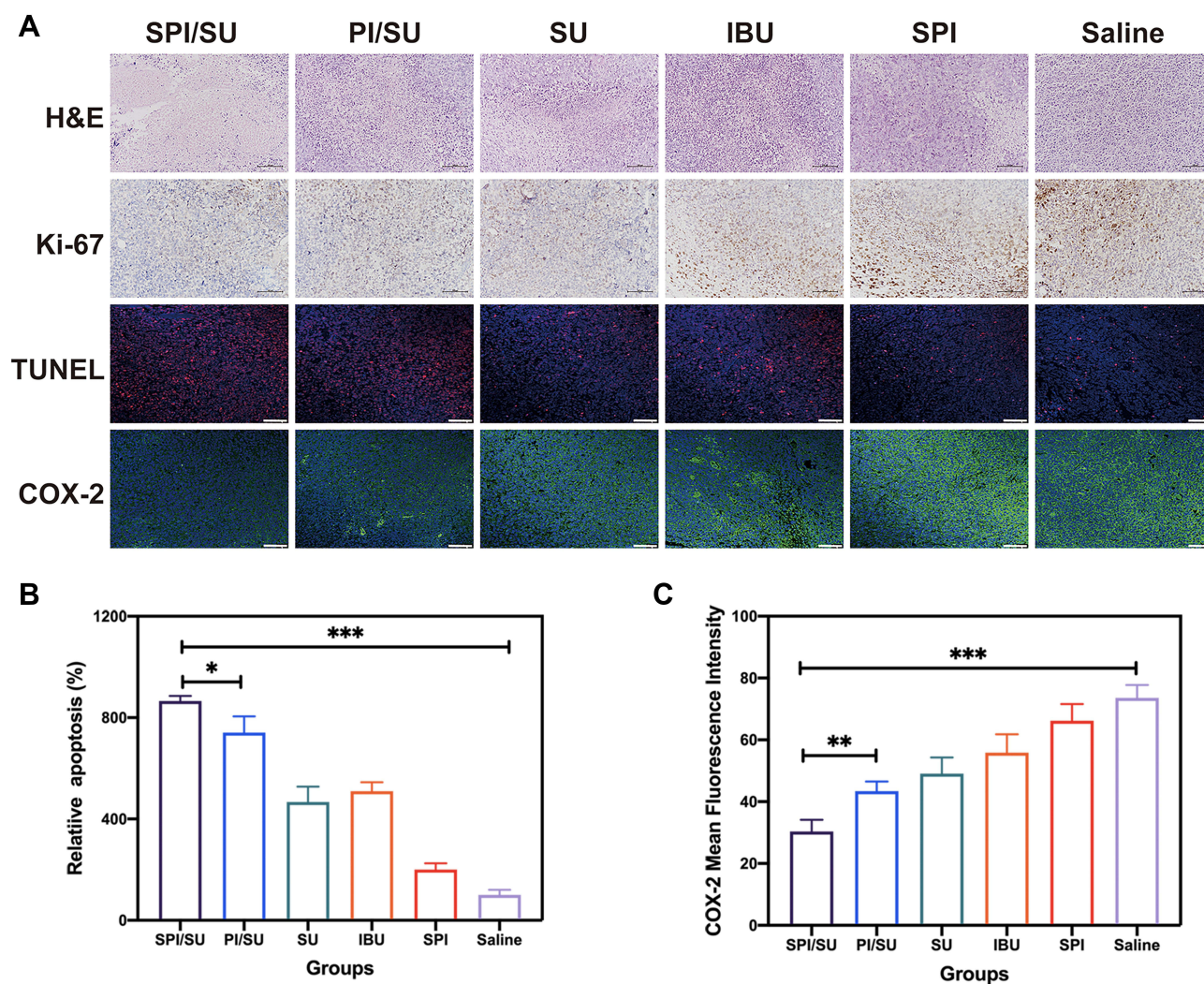**Abbreviation**: ns, not significant.

Figure 7 Histological analysis of isolated tumors. (**A**) Image of H&E assays and Ki-67 determination by immunochemistry, TUNEL assays and immunofluorescence analysis of xenograft tumors for COX-2 expression. The scale bar =50 μm (H&E and Ki-67), 25 μm (TUNEL and COX-2). (**B**) TUNEL measured by ImageJ software. (**C**) COX-2 immunofluorescence measured by ImageJ software. All data are mean ± SD, n=3. *$p < 0.05$, **$p < 0.01$, ***$p < 0.001$.

thrombocytopenia, which was attributed to the targeted delivery and release ability of SPI/SU nanomicelles at the tumor site (Figure 8B and C). Combined with former experimental results, it can be concluded that SPI/SU nanomicelles exhibit enhanced tumor treatment ability and weakened side effects in vivo.

Conclusion

In summary, we successfully designed and synthesized sialic acid-poly (ethylene glycol)-ibuprofen (SPI) nanomicelles that can effectively improve the efficiency of tumor inhibition attributed to E-selectin targeting. Moreover, the inhibition of COX-2 by ibuprofen affects the invasion and metastatic capabilities of tumor cells. As an "old drug" widely used in clinics, ibuprofen is endowed with the "new trick" of forming nanomicelles through conjugation. As a consequence, the SPI/SU nanomicelles exhibit enhanced tumor therapeutic effects. This research provides a new prospective to dig out traditional, efficient, and safe drugs in the treatment of cancer on innovative applications.
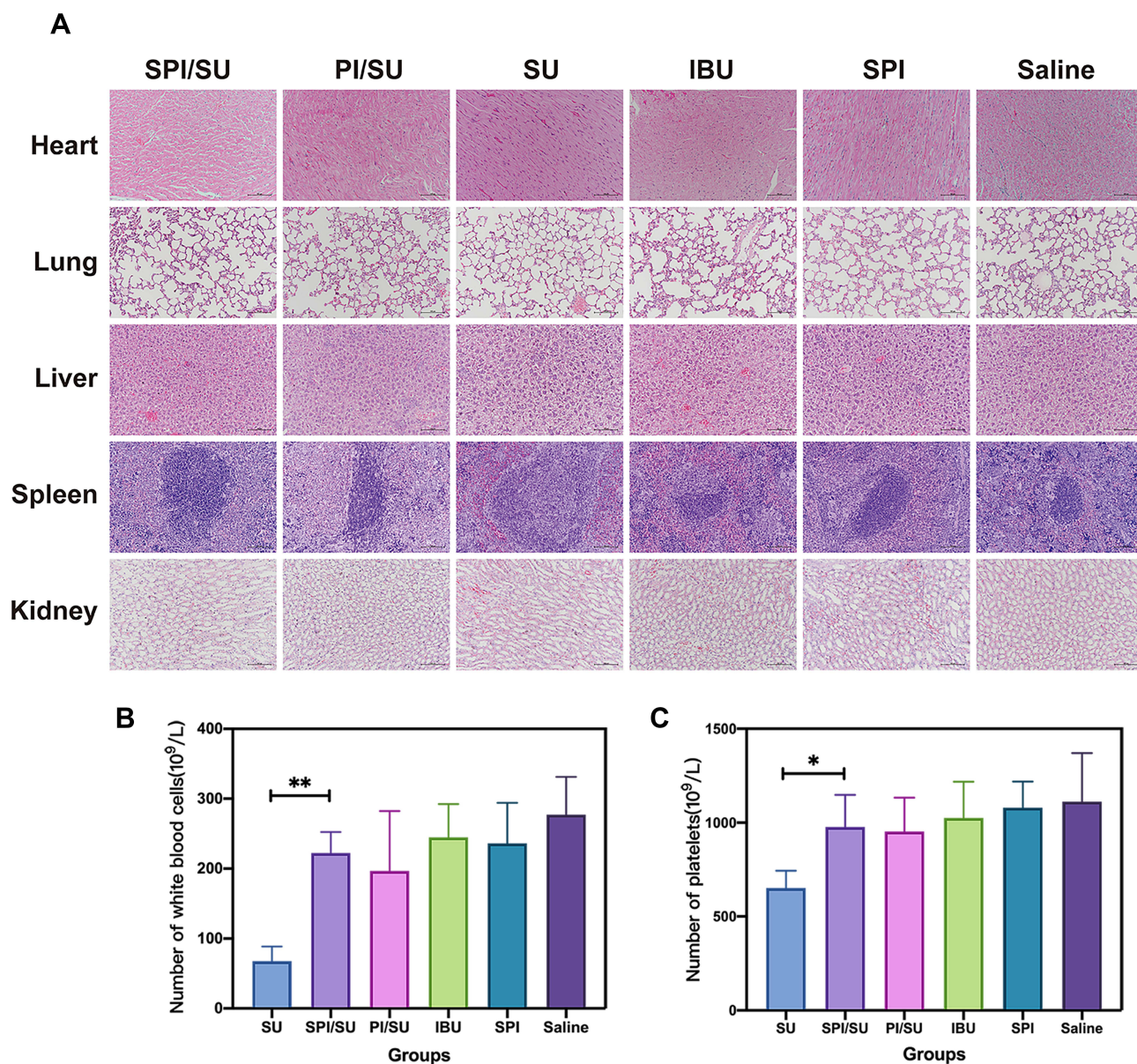
A

B

C

Figure 8 (**A**) H&E analysis of normal organs after various treatments. In H&E staining, nuclei are stained blue and the extracellular matrix and cytoplasm are stained red. (**B**) The number of white blood cells in the whole blood. (**C**) The number of platelets in the whole blood. All data are mean ± SD, n=3. *$p < 0.05$, **$p < 0.01$.

Animal Ethics Statement

BALB/c nude mice were provided by the Animal Experiment Center of Qingdao University. The study in vivo was performed under protocols approved by the Animal Management Rules of the Ministry of Health of the People's Republic of China (document no. 55, 2001) and the examination and approval of the Laboratory Animal Welfare Ethics Committee of Qingdao University (ethical approval number: 20220415BALB/cnude3520220615070).

Acknowledgments

Disclosure

The authors report no conflicts of interest in this work.

References

1. Nuñez KR. *Focus on Kidney Cancer Research*. New York: Nova Science; 2005.
2. Scelo G, Hofmann JN, Banks RE, et al. International cancer seminars: a focus on kidney cancer. *Ann Oncol*. 2016;27(8):1382–1385. doi:10.1093/annonc/mdw186
3. Weiss RH, Lin PY. Kidney cancer: identification of novel targets for therapy. *Kidney Int*. 2006;69(2):224–232. doi:10.1038/sj.ki.5000065
4. Thoma C. Kidney cancer: combining targeted and immunotherapy. *Nat Rev Urol*. 2018;15(5):263.
5. Chen HX, Cleck JN. Adverse effects of anticancer agents that target the VEGF pathway. *Nat Rev Clin Oncol*. 2009;6(8):465–477. doi:10.1038/nrclinonc.2009.94
6. Bex A, Powles T, Haanen J. Sunitinib alone or after nephrectomy in renal cancer. *N Engl J Med*. 2018;379(19):1877–1878.
7. Bex A. Adjuvant sunitinib in renal cell carcinoma: from evidence to recommendation. *Ann Oncol*. 2017;28(4):682–684. doi:10.1093/annonc/mdx014
8. Wei G, Sun H, Dong K, et al. The thermogenic activity of adjacent adipocytes fuels the progression of ccRCC and compromises anti-tumor therapeutic efficacy. *Cell Metab*. 2021;33(10):2021–2039. doi:10.1016/j.cmet.2021.08.012
9. Mejean A, Ravaud A, Thezenas S, et al. Sunitinib alone or after nephrectomy for patients with metastatic renal cell carcinoma: is there still a role for cytoreductive nephrectomy? *Eur Urol*. 2021;80(4):417–424. doi:10.1016/j.eururo.2021.06.009
10. Czarnecka AM. Intermittent sunitinib is an effective renal carcinoma treatment. *Nat Rev Urol*. 2017;14(5):264–266. doi:10.1038/nrurol.2017.36
11. Blay JY. Pharmacological management of gastrointestinal stromal tumours: an update on the role of sunitinib. *Ann Oncol*. 2010;21(2):208–215. doi:10.1093/annonc/mdp291
12. Chu TF, Rupnick MA, Kerkela R, et al. Cardiotoxicity associated with tyrosine kinase inhibitor sunitinib. *Lancet*. 2007;370(9604):2011–2019. doi:10.1016/S0140-6736(07)61865-0
13. Brzezniak C, Szabo E. Images in clinical medicine. Sunitinib-associated hair depigmentation. *N Engl J Med*. 2014;370(17):e27. doi:10.1056/NEJMicm1309906
14. Poprach A, Pavlik T, Melichar B, et al. Skin toxicity and efficacy of sunitinib and sorafenib in metastatic renal cell carcinoma: a national registry-based study. *Ann Oncol*. 2012;23(12):3137–3143. doi:10.1093/annonc/mds145
15. Lacouture ME, Reilly LM, Gerami P, Guitart J. Hand foot skin reaction in cancer patients treated with the multikinase inhibitors sorafenib and sunitinib. *Ann Oncol*. 2008;19(11):1955–1961. doi:10.1093/annonc/mdn389
16. Hwang D, Ramsey JD, Kabanov AV. Polymeric micelles for the delivery of poorly soluble drugs: from nanoformulation to clinical approval. *Adv Drug Deliver Rev*. 2020;156:80–118.
17. Duncan R. Polymer therapeutics: top 10 selling pharmaceuticals - what next? *J Control Release*. 2014;190:371–380. doi:10.1016/j.jconrel.2014.05.001
18. Ghosh B, Biswas S. Polymeric micelles in cancer therapy: state of the art. *J Control Release*. 2021;332:127–147. doi:10.1016/j.jconrel.2021.02.016
19. Ghezzi M, Pescina S, Padula C, et al. Polymeric micelles in drug delivery: an insight of the techniques for their characterization and assessment in biorelevant conditions. *J Control Release*. 2021;332:312–336. doi:10.1016/j.jconrel.2021.02.031
20. Zhang M, Zhao Y, Ma H, Sun Y, Cao J. How to improve photodynamic therapy-induced antitumor immunity for cancer treatment? *Theranostics*. 2022;12(10):4629–4655. doi:10.7150/thno.72465
21. Schulz M, Salamero-Boix A, Niesel K, Alekseeva T, Sevenich L. Microenvironmental regulation of tumor progression and therapeutic response in brain metastasis. *Front Immunol*. 2019;10:1713. doi:10.3389/fimmu.2019.01713
22. Jain S, Chakraborty G, Kundu GC. The crucial role of cyclooxygenase-2 in osteopontin-induced protein kinase C alpha/c-Src/IkappaB kinase alpha/beta-dependent prostate tumor progression and angiogenesis. *Cancer Res*. 2006;66(13):6638–6648. doi:10.1158/0008-5472.CAN-06-0661
23. Menter DG, Schilsky RL, DuBois RN. Cyclooxygenase-2 and cancer treatment: understanding the risk should be worth the reward. *Clin Cancer Res*. 2010;16(5):1384–1390. doi:10.1158/1078-0432.CCR-09-0788
24. St-Germain ME, Gagnon V, Parent S, Asselin E. Regulation of COX-2 protein expression by Akt in endometrial cancer cells is mediated through NF-kappa B/I kappa B pathway. *Mol Cancer*. 2004;3:7. doi:10.1186/1476-4598-3-7
25. Young LE, Sanduja S, Bemis-Standoli K, et al. The mRNA binding proteins hur and tristetraprolin regulate cyclooxygenase 2 expression during colon carcinogenesis. *Gastroenterology*. 2009;136(5):1669–1679. doi:10.1053/j.gastro.2009.01.010
26. Sheng HM, Shao JY, Kirkland SC, et al. Inhibition of human colon cancer cell growth by selective inhibition of cyclooxygenase-2. *J Clin Invest*. 1997;99(9):2254–2259. doi:10.1172/JCI119400
27. Garg R, Blando JM, Perez CJ, et al. COX-2 mediates pro-tumorigenic effects of PKCepsilon in prostate cancer. *Oncogene*. 2018;37(34):4735–4749. doi:10.1038/s41388-018-0318-9
28. Zhang G, Panigrahy D, Hwang SH, et al. Dual inhibition of cyclooxygenase-2 and soluble epoxide hydrolase synergistically suppresses primary tumor growth and metastasis. *Proc Natl Acad Sci USA*. 2014;111(30):11127–11132. doi:10.1073/pnas.1410432111
29. Ko CJ, Lan SW, Lu YC, et al. Inhibition of cyclooxygenase-2-mediated matriptase activation contributes to the suppression of prostate cancer cell motility and metastasis. *Oncogene*. 2017;36(32):4597–4609. doi:10.1038/onc.2017.82
30. Rozic JG, Chakraborty C, Lala PK. Cyclooxygenase inhibitors retard murine mammary tumor progression by reducing tumor cell migration, invasiveness and angiogenesis. *Int J Cancer*. 2001;93(4):497–506. doi:10.1002/ijc.1376
31. Wang D, Cabalag CS, Clemons NJ, DuBois RN. Cyclooxygenases and prostaglandins in tumor immunology and microenvironment of gastrointestinal cancer. *Gastroenterology*. 2021;161(6):1813–1829. doi:10.1053/j.gastro.2021.09.059
32. Scartozzi M, Galizia E, Freddari F, et al. Molecular biology of sporadic gastric cancer: prognostic indicators and novel therapeutic approaches. *Cancer Treat Rev*. 2004;30(5):451–459. doi:10.1016/j.ctrv.2004.01.001
33. Doogan DP. Topical non-steroidal anti-inflammatory drugs. *Lancet*. 1989;2(8674):1270–1271. doi:10.1016/S0140-6736(89)91869-2
34. Harris RE, Beebe-Donk J, Doss H, Doss DB. Aspirin, ibuprofen, and other non-steroidal anti-inflammatory drugs in cancer prevention: a critical review of non-selective COX-2 blockade (review). *Oncol Rep*. 2005;13(4):559–583.

35. Hu JB, Kang XQ, Liang J, et al. E-selectin-targeted sialic acid-PEG-dexamethasone micelles for enhanced anti-inflammatory efficacy for acute kidney injury. *Theranostics*. 2017;7(8):2204–2219. doi:10.7150/thno.19571

36. Lunemann JD, von Gunten S, Neumann H. Targeting sialylation to treat central nervous system diseases. *Trends Pharmacol Sci*. 2021;42 (12):998–1008. doi:10.1016/j.tips.2021.09.002

37. Grun MK, Suberi A, Shin K, et al. PEGylation of poly (amine-co-ester) polyplexes for tunable gene delivery. *Biomaterials*. 2021;272. doi:10.1016/j.biomaterials.2021.120780

38. Wang HX, Xie HY, Wu JP, et al. Structure-based rational design of prodrugs to enable their combination with polymeric nanoparticle delivery platforms for enhanced antitumor efficacy. *Angew Chem Int Edit*. 2014;53(43):11532–11537. doi:10.1002/anie.201406685

39. Yongvongsoontorn N, Chung JE, Gao SJ, et al. Carrier-enhanced anticancer efficacy of sunitinib-loaded green tea-based micellar nanocomplex beyond tumor-targeted delivery. *Acs Nano*. 2019;13(7):7591–7602. doi:10.1021/acsnano.9b00467

40. Song HJ, Su Q, Shi WF, et al. Antigen epitope-TLR7/8a conjugate as self-assembled carrier-free nanovaccine for personalized immunotherapy. *Acta Biomater*. 2022;141:398–407. doi:10.1016/j.actbio.2022.01.004

41. Jafari H, Mahdavinia GR, Kazemi B, et al. Highly efficient sunitinib release from pH-responsive mHPMC@Chitosan core-shell nanoparticles. *Carbohydr Polym*. 2021;258:117719. doi:10.1016/j.carbpol.2021.117719

42. Liang CH, Bai XY, Qi CL, et al. Pi electron-stabilized polymeric micelles potentiate docetaxel therapy in advanced-stage gastrointestinal cancer. *Biomaterials*. 2021;266:120432. doi:10.1016/j.biomaterials.2020.120432

43. Zhang Y, Zhang BT, Teng YG, Zhao JJ, Sun XJ. Heterogeneous activation of persulfate by carbon nanofiber supported Fe3O4@carbon composites for efficient ibuprofen degradation. *J Hazard Mater*. 2021;401:1.

44. Abbasi Kajani A, Bordbar AK. Biogenic magnetite nanoparticles: a potent and environmentally benign agent for efficient removal of azo dyes and phenolic contaminants from water. *J Hazard Mater*. 2019;366:268–274. doi:10.1016/j.jhazmat.2018.11.111

45. Zhu C, Han S, Zeng X, et al. Multifunctional thermo-sensitive hydrogel for modulating the microenvironment in Osteoarthritis by polarizing macrophages and scavenging RONS. *J Nanobiotechnology*. 2022;20(1):221. doi:10.1186/s12951-022-01422-9

46. Song HJ, Huang PS, Niu JF, et al. Injectable polypeptide hydrogel for dual-delivery of antigen and TLR3 agonist to modulate dendritic cells in vivo and enhance potent cytotoxic T-lymphocyte response against melanoma. *Biomaterials*. 2018;159:119–129. doi:10.1016/j.biomaterials.2018.01.004

47. Xu J, Ma Q, Zhang Y, et al. Yeast-derived nanoparticles remodel the immunosuppressive microenvironment in tumor and tumor-draining lymph nodes to suppress tumor growth. *Nat Commun*. 2022;13(1):110. doi:10.1038/s41467-021-27750-2

48. Bazylinska U, Wawrzynczyk D, Kulbacka J, et al. Hybrid theranostic cubosomes for efficient NIR-induced photodynamic therapy. *Acs Nano*. 2022;16(4):5427–5438. doi:10.1021/acsnano.1c09367

49. Huang XL, Teng X, Chen D, Tang FQ, He JQ. The effect of the shape of mesoporous silica nanoparticles on cellular uptake and cell function. *Biomaterials*. 2010;31(3):438–448. doi:10.1016/j.biomaterials.2009.09.060

50. Zang XL, Song JX, Li YF, Han YT. Targeting necroptosis as an alternative strategy in tumor treatment: from drugs to nanoparticles. *J Control Release*. 2022;349:213–226. doi:10.1016/j.jconrel.2022.06.060

51. Li Yanfeng ZX, Jinxiao S, Xie Y, Xuedong C, Chen X. pH/ROS dual-responsive nanoparticles with curcumin entrapment to promote antitumor efficiency in triple negative breast cancer. *J Drug Deliv Sci Technol*. 2022;74:103520. doi:10.1016/j.jddst.2022.103520

52. Daneau G, Boidot R, Martinive P, Feron O. Identification of cyclooxygenase-2 as a major actor of the transcriptomic adaptation of endothelial and tumor cells to cyclic hypoxia: effect on angiogenesis and metastases. *Clin Cancer Res*. 2010;16(2):410–419. doi:10.1158/1078-0432.CCR-09-0583

53. Liu JF, Fong YC, Chang CS, et al. Cyclooxygenase-2 enhances alpha2beta1 integrin expression and cell migration via EP1 dependent signaling pathway in human chondrosarcoma cells. *Mol Cancer*. 2010;9:43. doi:10.1186/1476-4598-9-43

54. Zarbock A, Lowell CA, Ley K. Spleen tyrosine kinase syk is necessary for E-Selectin-induced alpha (L) beta 2 integrin-mediated rolling on intercellular adhesion molecule-1. *Immunity*. 2007;26(6):773–783. doi:10.1016/j.immuni.2007.04.011

55. Li KK, Zang XL, Meng XJ, et al. Targeted delivery of quercetin by biotinylated mixed micelles for non-small cell lung cancer treatment. *Drug Deliv*. 2022;29(1):970–985. doi:10.1080/10717544.2022.2055225

56. Zang X, Song J, Yi X, Piyu J. Polymeric indoximod based prodrug nanoparticles with doxorubicin entrapment for inducing immunogenic cell death and improving the immunotherapy of breast cancer. *J Mater Chem B*. 2022;10(12):2019–2027. doi:10.1039/D2TB00197G

57. Dudderidge TJ, Stoeber K, Loddo M, et al. Mcm2, Geminin, and Ki67 define proliferative state and are prognostic markers in renal cell carcinoma. *Clin Cancer Res*. 2005;11(7):2510–2517. doi:10.1158/1078-0432.CCR-04-1776

58. Blankenberg FG, Levashova Z, Goris MG, et al. Targeted systemic radiotherapy with scVEGF/ 177 Lu leads to sustained disruption of the tumor vasculature and intratumoral apoptosis. *J Nucl Med*. 2011;52(10):1630–1637. doi:10.2967/jnumed.111.091629

59. Wang MZ, Niu J, Ma HJ, et al. Transdermal siRNA delivery by pH-switchable micelles with targeting effect suppress skin melanoma progression. *J Control Release*. 2020;322:95–107. doi:10.1016/j.jconrel.2020.03.023